# Negative cooperativity exhibited by the lytic amino-terminal domain of human perforin: implications for perforin-mediated cell lysis

**N Rochel and JA Cowan***

Department of Chemistry, The Ohio State University, 120 West 18th Avenue, Columbus, OH 43210, USA

**Background:** Cytolytic effector cells of the immune system recognize and lyse cells that carry non-self epitopes. One mechanism of cell lysis involves release of a 67-kDa pore-forming protein, perforin. The amino-terminal domain of perforin (≥19 residues) can account for most of the lysis activity, by a mechanism that is similar to that of holoperforin. Detailed mechanistic studies of this domain should yield useful insight into the factors underlying perforin activity *in vivo*.

**Results:** The mechanism of pore formation by the 22-residue amino-terminal domain of perforin was studied by kinetic and thermodynamic methods. Approximately $4 \pm 1$ peptide monomers form an active pore by a mechanism that displays negative cooperativity.

**Conclusions:** A negatively-regulated aggregation mechanism is likely to be common for pore-forming peptides. The positively-charged domain B of perforin (residues 7–15) may mediate cooperativity through electrostatic interactions. Such a mechanism limits the number of protein molecules that are committed to any particular channel. This data supports smaller pores as the physiologically relevant aggregate, rather than the larger ring sizes identified by electron microscopy at higher, non-biological concentrations.

**Chemistry & Biology** January 1996, **3**:31–36

Key words: cytolysis, kinetics, negative cooperativity, perforin

## Introduction

Cytotoxic T lymphocytes (CTL) are effector cells of the immune system that recognize and lyse target cells carrying non-self epitopes [1,2]. CTL's appear to mediate cell lysis by two distinct pathways (Fig. 1). The first pathway results in the release of perforin, a 67-kDa pore-forming protein that shows significant homology to the ninth component (C9) of human complement [3]; the second involves surface-bound Fas ligands and receptors [2,4,5]. Recent investigations have demonstrated that most of the lysis activity of human (or murine) perforin can be accounted for by a 19-residue amino-terminal peptide, by a mechanism that is similar to that of holoperforin [6,7]. Detailed structural and mechanistic studies of this domain should therefore yield useful insight into the factors underlying perforin activity *in vivo*. The studies reported here address the mechanism of pore formation by the 22-residue amino-terminal domain of perforin ($P_{22}$), which includes the tryptophan residue at position 21 as a fluorescent probe [8]. We have found that the amino-terminal peptide mediates lysis of a target membrane by a mechanism that exhibits a high degree of negative cooperativity. Peptide binding was analyzed in terms of a model that incorporates non-ideal interactions and aggregation in a membrane bilayer. The minimum number of peptide monomers required to form an active pore was estimated to be $\sim 4 \pm 1$. Negative regulation of pore formation is likely to be mediated by a positively-charged sequence of residues in the amino-terminal domain.

Positively cooperative binding phenomena are more commonly observed in biological chemistry and range from the well characterized example of dioxygen binding to hemoglobin, to the stacking of nucleotide bases and the formation of aggregates of indefinite size [9]. Negative cooperativity is characterized by those cases where binding of a ligand to a protein decreases the affinity of the protein for other ligands of the same or a different type. For example, negative cooperativity is observed in the binding of aspartates to aspartate receptors [10]. Binding of the first aspartate induces a change of conformation that diminishes the affinity for binding of a second ligand. Negative cooperativity is also observed in the binding of nucleotides by helicase Dna B [11]. In our case, negative cooperativity is observed during the peptide aggregation step of pore formation, where the ligand is an additional peptide molecule, and electrostatic interactions among these peptides appear to limit the size of the pore.

## Results and discussion

Assembly of the active pore complex was assayed spectrophotometrically by monitoring the release of carboxyfluorescein (CF) from synthetic vesicles composed of phosphatidylcholine (PC) and cholesterol (1:1) (Figs 2,3) [6]. Since the size and uniformity of vesicle preparations are important factors that influence the rate of CF release [12], we have prepared uniform small unilamellar vesicles by use of a sonication method [13]. This method provides small homogeneous vesicles with diameters of

*Corresponding author.

 ISSN 1074-5521

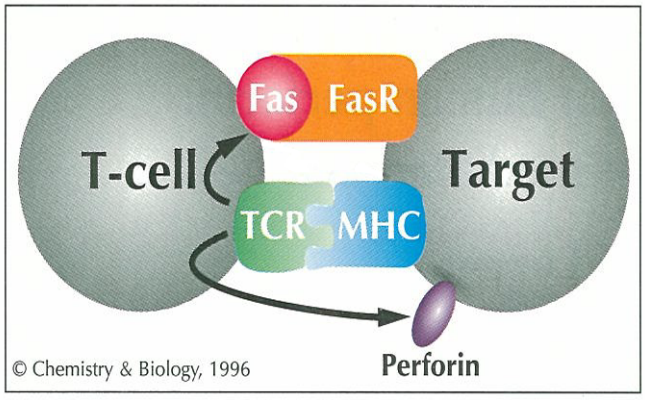


**Fig. 1.** Summary of CTL-mediated pathways. After binding of the major histocompatibility complex (MHC) to the T-cell receptor (TCR), perforin is released from the T-cell, and/or Fas ligand is expressed. The latter may form a complex with the Fas receptor (FasR) on the target cell membrane to initiate an apoptotic response.

~40 ± 10 nm, as determined by electron microscopy, although the encapsulation efficiency is reduced as a consequence of the smaller internal volume.

Kinetic data were analyzed in terms of a model that describes pore formation as a two-step process: partitioning of the peptide into the membrane, followed by aggregation to form a functional pore [14,15]. The kinetic scheme can be described by the following equations:

$$A_f + L \underset{}{\overset{\text{fast}}{\rightleftharpoons}} A_l \qquad (1)$$

$$m\,A_l \longrightarrow R \qquad (2)$$

where $A_f$ is the free aqueous peptide, $A_l$ is the monomeric, lipid-associated peptide, L is a lipid membrane, and m is the number of peptide monomers that form a pore R. Release of carboxyfluorescein is diffusion-controlled once the pore is formed. Since the lifetime of the pore is longer than the time necessary for complete diffusive efflux of the dye (as estimated from Fick's law), pore formation meets the requirement for complete release of the dye. The first step, which involves partitioning of the monomeric peptide inside the membrane, is very fast for the pore-forming peptide melittin ($1.4 \times 10^5\ M^{-1}\ s^{-1}$) [16]. Since the time taken for the first step of pore formation by $P_{22}$ is likely to be similar to that taken by melittin, partitioning of $P_{22}$ should be complete in seconds. The time required for lysis is on the order of minutes; we associate this slow rate with the $P_{22}$ aggregation step after membrane insertion. An alternative mechanism, where the peptide simply serves to disrupt the membrane without pore formation, is inconsistent with the slow rate of release of CF.

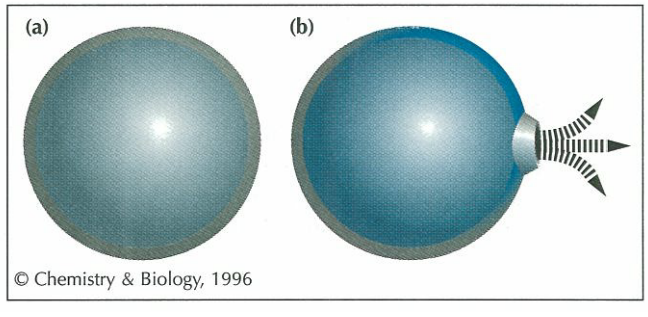


**Fig. 2.** Schematic illustration of the assay for monitoring pore formation using carboxyfluorescein filled vesicles. **(a)** The concentrated dye solution (80 mM) shows weak fluorescence as a result of self-quenching. **(b)** After addition of the peptide, a pore is formed and carboxyfluorescein is rapidly released from the vesicle. Upon dilution of carboxyfluorescein, the fluorescence intensity increases.

Within the framework of this model, the measure p(t), the average number of pores per vesicle at time t, can be

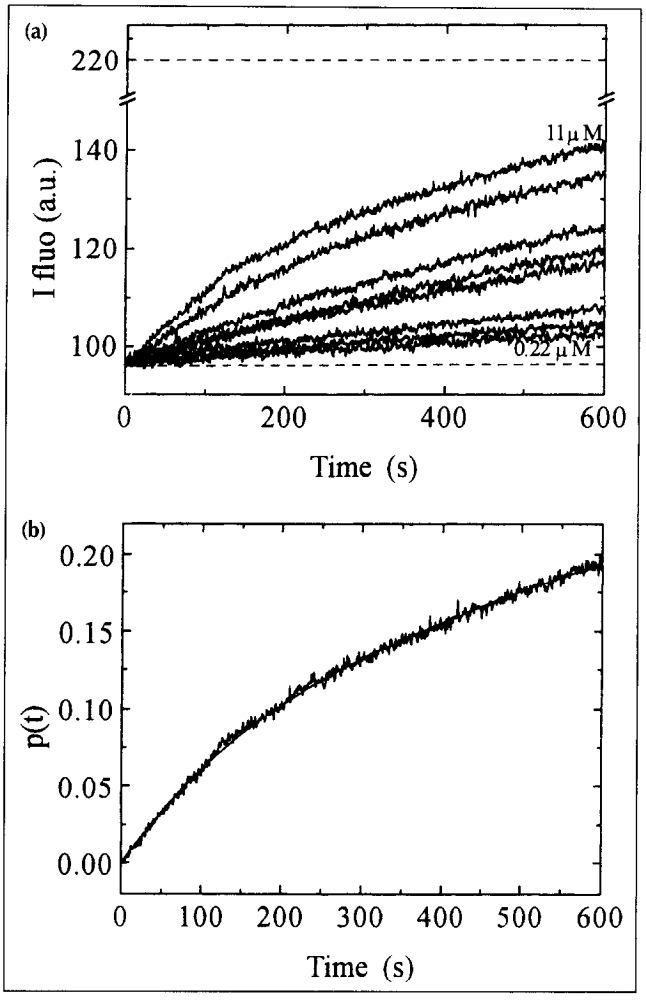


**Fig. 3.** Steady-state kinetic traces of pore formation. **(a)** Time trace showing the change in fluorescence intensity as a function of peptide concentration (0.22, 0.44, 0.55, 1.00, 2.21, 3.32, 8.3 and 11.0 μM) after mixing with carboxyfluorescein-entrapped vesicles (phosphatidylcholine:cholesterol, 1:1, lipid concentration 1 mM). For the data shown, a pH gradient ($pH_{inside} = 5.0$, $pH_{outside} = 7.0$) was used to accentuate the change in carboxyfluorescein emission. The upper dashed line corresponds to the limiting ($F_\infty$) value obtained after addition of Triton X-100 (0.02 % final concentration). The background rate of CF release in the absence of $P_{22}$ is indicated by the lower dashed line. **(b)** Plot of p(t), the average number of pores per vesicle at time t, versus time, for peptide and lipid concentrations of 11 μM and 1 mM, respectively. The solid curve through the data was calculated according to equation 4.

related to the change in carboxyfluorescein emission using equation 3 [14],

$$p(t) = -\ln (F_\infty - F(t))/(F_\infty - F_o) \quad (3)$$

where F(t) is the observed fluorescence intensity at time t, $F_\infty$ is the final limiting fluorescence, and $F_o$ is the initial fluorescence of the intact vesicles. Figure 3b shows the plot of p(t) versus time. The rate profile for association decreases from an initial fast rate ($v_{p0}$) that is limited only by the rate of pore formation, to an intermediate value ($v_{pi}$) that results in a steady-state release of carboxyfluorescein. The latter results from a variety of factors that include the size distribution of the vesicles, inactivation of pore formation with time, and possibly rate-limiting dissociation and re-employment of the peptide. A correction that accounts for the size distribution of vesicles can be applied to the p(t) function; however, both this, and the other factors just detailed, are negligible in the early stages of the plot, which is used to determine the initial velocity $v_{p0}$ [14,15]. For this reason they can be reasonably neglected for this analysis. The kinetic profile shown in Figure 3 can be fit to equation 4 [14], with a time constant (k).

$$p(t) = v_{pi}\, t + (v_{p0} - v_{pi})[(1 - e^{-kt})/k] \quad (4)$$

Figure 4a shows the result of a Hill analysis of the initial rate ($v_{p0}$) [17]. A fit to the linear portion of the plot gave a Hill coefficient $h = 0.72 \pm 0.08$, indicative of negative cooperativity. In Figure 4b, a plot of $1/v_{p0}$ versus $1/[P_{22}]$ shows a concave-down profile, again characteristic of negative cooperativity [17]. These data were obtained with a pH gradient ($pH_{inside} = 5.0$, $pH_{outside} = 7.0$) to accentuate the change in carboxyfluorescein emission. Negative cooperativity was also observed in the absence of a gradient ($pH_{inside} = 7.0$, $pH_{outside} = 7.0$), although the change in emission was smaller and the errors were greater (Figs. 4c,d).

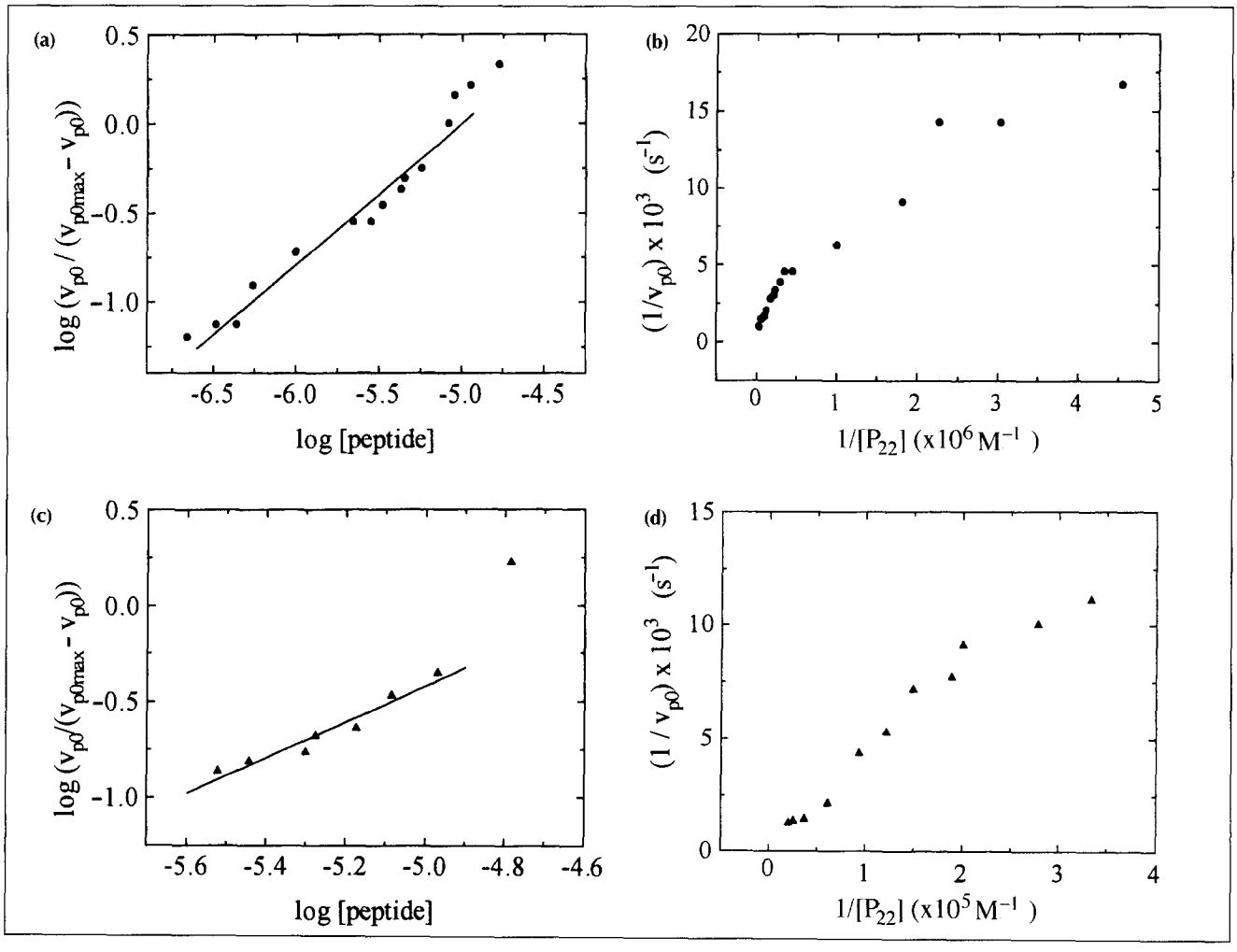


**Fig. 4.** A Hill analysis indicates negative cooperativity. **(a)** The results of a Hill analysis of the initial rate data for peptide-mediated release of carboxyfluorescein from lipid vesicles (experimental conditions as described in the legend to Fig. 3), and **(b)** the variation of $1/v_{p0}$ versus $1/[P_{22}]$. The value of $v_{p0max}$ was calculated from the intercept of a plot of $1/v_{p0}$ vs $1/[peptide]_0$ [17]. A Hill coefficient $h = 0.72$ was obtained. These results were confirmed by independent monitoring of the change in fluorescence intensity of the tryptophan residue accompanying binding and pore formation. Titrations were carried out both by adding vesicles to a solution of peptide, and by adding increasing amounts of peptide to a solution of vesicles. For comparison, **(c)** and **(d)** show the results of a similar Hill analysis for data obtained in the absence of a pH gradient ($pH_{inside} = 7.0$, $pH_{outside} = 7.0$). A Hill coefficient $h = 0.9$ was obtained.

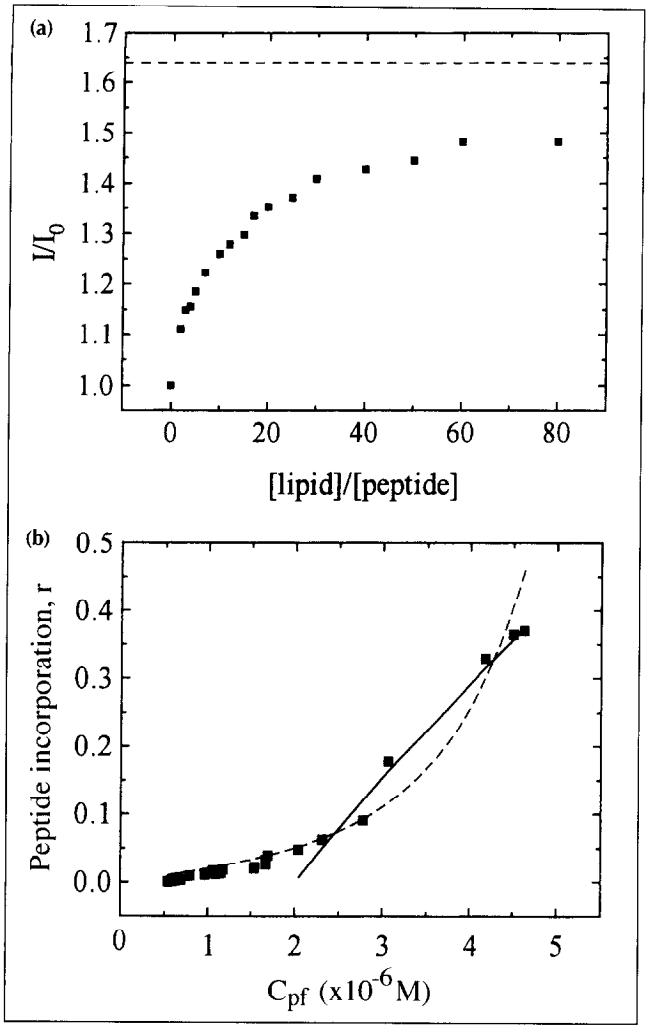


**Fig. 5.** Evaluation of the number of peptide monomers required to form an active pore. **(a)** Increase of the tryptophan fluorescence ($I/I_0$) at 355 nm for 17 μM peptide upon titration with lipid vesicles (phosphatidylcholine:cholesterol, 1:1, lipid concentration between 34 μM and 1.4 mM) in Hepes buffer (10 mM) with NaCl (150 mM) at 25 °C. Data were obtained in the absence of a pH gradient ($pH_{inside} = 7.0$, $pH_{outside} = 7.0$). Fluorescence intensities were corrected using the vesicle blank. The upper dashed line corresponds to the limiting value of $I/I_0$ calculated from double-reciprocal plots according to standard procedures [18,19]. **(b)** Plot of the degree of incorporation of the peptide (r) versus free peptide concentration ($C_{pf}$). The solid line shows a fit of the data at high r values to equation 5 (with $C_{pf}^* = 2.0$ μM and $z = 1.5$), and the dashed line corresponds to a fit of the data at low r values to equation 6, which accommodates cooperativity (with $C_{pf}^* = 2.0$ μM, $z = 1.5$, $B = 20$, and $m = 4$).

Supporting evidence for negative cooperativity was also obtained from thermodynamic binding studies by monitoring the intrinsic fluorescence of tryptophan 21 (Fig. 5a). Fitting the binding data by a simple Hill analysis provided a coefficient $h = 0.8 \pm 0.1$. In addition, cooperativity is clearly demonstrated by the analysis of these data shown in Figure 5b and discussed below.

To obtain a more representative view of pore formation, a model (shown schematically in Fig. 6) that includes monomer partitioning, aggregation, and thermodynamic non-ideality was considered [18,19]. This model assumes

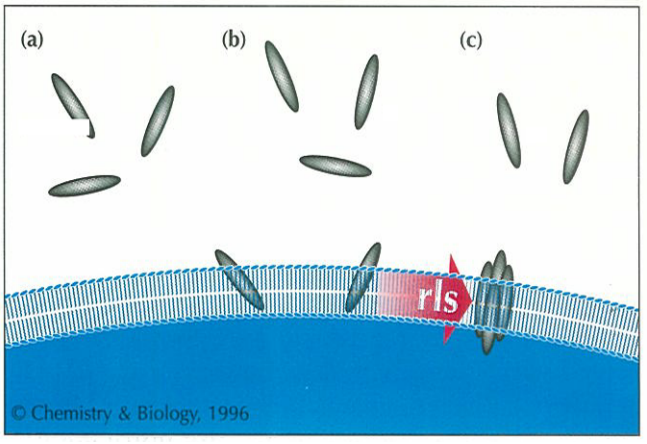


**Fig. 6.** Three key steps to pore formation. **(a)** The peptide concentration must reach a critical level $C_{pf}^*$ before significant partitioning into the lipid membrane **(b)** and aggregation **(c)** can occur. At this point the partition constant, Γ (a type of equilibrium constant) defines the relative concentration of free ($C_{pf}$) and membrane-associated ($C_{pa}$) peptide. Subsequently, m peptide monomers aggregate in a rate-limiting step (rls) to form an active pore (c). The aggregation occurs in a negatively cooperative manner.

that there is no aggregation of the peptide in the aqueous phase. This assumption is justified by results from NMR experiments, which show no evidence for peptide aggregation even at higher concentrations than those used in these studies. Figure 5a shows the increase of the Trp fluorescence intensity ratio $I/I_o$ at 355 nm upon titration with lipid vesicles, where I is the observed fluorescence intensity, and $I_o$ is the control intensity in the absence of lipid. The total concentration of peptide ($C_p$) is equal to the sum of the free peptide concentration ($C_{pf}$) and the lipid-associated peptide concentration ($C_{pa}$) (Fig. 6), while the extent of incorporation (r) is equal to $C_{pa}/C_l$ where $C_l$ is the lipid concentration. The magnitudes of r and $C_{pf}$ were calculated by standard procedures [16,18,19], and the extent of association defined by a plot of r versus $C_{pf}$ is shown in Figure 5b. The initial lag phase and subsequent upward turn are again characteristic of a cooperative process [19].

Assuming a two-state model, the fluorescence intensity ratio is proportional to r through the relationship $I/I_0 = (I/I_0)_\infty . r.C_l/C_p$. The shape of the plot in Figure 5b is consistent with the model illustrated in Figure 6, involving the partitioning of monomeric peptide, followed by aggregation within the membrane. Simple binding would result in a straight line plot of r versus $C_{pf}$, rather than the curve that is actually observed, with an early lag phase and subsequent rise after the critical free peptide concentration, $C_{pf}^*$, is reached [18,19]. This mechanistic model has been successful in rationalizing the behavior of a number of peptides, including paradaxin [20] and the α5 segment of δ-endotoxin [21].

The partition coefficient, which provides a measure of the affinity of the peptide for the membrane, was calculated for the monomeric peptide $P_{22}$ ($\Gamma = 10^3 M^{-1}$) from the very beginning of the lag phase, with the extent of incorporation of the monomeric peptide defined by

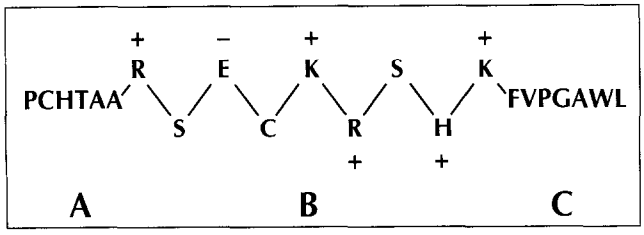


**Fig. 7.** Domain structure of the perforin peptide. Electrostatic repulsion between multiple copies of the positively charged central domain B may be responsible for the negative cooperativity associated with pore formation.

$r_1 = \Gamma_1 C_{pf}$. This value is of the same order of magnitude as the partition coefficient of the channel-forming alamethicin peptide ($\Gamma = 10^3\ M^{-1}$) [18], but is one order of magnitude smaller than the coefficient for melittin ($\Gamma = 3 \times 10^4\ M^{-1}$) [16], a strong surface-binding peptide. A sharp upwards turn is observed at the critical concentration $C_{pf}^*$, at which the peptide aggregates in the membrane. For larger values of r (> 0.05), corresponding to $[P_{22}] > C_{pf}^*$, essentially all of the incorporated peptide is aggregated. Under these conditions, equation 5 holds [18], where z is a numerical constant.

$$C_{pf} = (1 + 2r)^z C_{pf}^* \quad (5)$$

A fit of our data to this equation for values of $r > 0.1$ provides a value of 2.0 μM for $C_{pf}^*$ and 1.5 for z. This model does not, however, fit the lag part of the curve (Fig. 5b). At peptide concentrations that are less than the critical concentration $C_{pf}^*$ ($[P_{22}] < 2\,\mu M$), equation 6 is appropriate [18], where B is an equilibrium constant that relates to addition of a membrane-bound monomer to the aggregate, $s = (C_{pf}/C_{pf}^*)/(1 + 2r)^z$ and m is the number of monomers that form a pore [18]. Satisfactory fits were obtained when m was in the range of 3 to 5.

$$Br = s[1 + \{(m(1 - s) + s)s^{(m-1)}/(1 - s)^2\}] \quad (6)$$

This model assumes an isodesmic aggregation, where each aggregation step is assumed to have the same equilibrium constant B. While other models can be used, the resulting fit to the data shows no difference in comparison to the isodesmic model. The fit to the data with equation 6 provides reasonable parameters and lends credence to the model.

It is important to note that this data supports a previous proposal that smaller pores are the physiologically relevant aggregate in perforin-mediated target cell lysis [2], rather than the larger ring sizes that have been identified by electron microscopy. The latter data are obtained under conditions of higher concentration that may not be relevant in a biological context.

The primary sequence of the peptide suggests a functional model whereby the strongly positively charged domain B (residues 7–15; Fig. 7) may negatively regulate cooperativity though electrostatic interactions among the charged sidechains. This is supported by the lower cooperativity observed at moderately higher pH (Fig. 4c,d). Such a model is open to experimental testing and studies of this nature are currently underway in our laboratory.

## Significance

**We have demonstrated a significant level of negative cooperativity in peptide aggregation and pore formation for the lytic amino-terminal domain of perforin. To our knowledge there have been no prior reports of negative cooperativity in pore formation by such peptides. However, a negatively-regulated aggregation mechanism is likely to be common for pore-forming peptides, and is reasonable in view of the functional requirements of the perforin protein, providing a mechanism to limit the number of protein molecules that are committed to any particular channel. These data also support the notion that a small pore size is the physiologically relevant aggregate in perforin-mediated cell lysis, not the larger ring sizes identified by electron microscopy at higher, non-biological, concentrations of perforin [2].**

## Materials and methods

### *Peptide synthesis and modification*

The 22-residue peptide was prepared by automated synthesis in The Ohio State Biochemical Instrument Center on a Beckman F308 peptide synthesizer, and purified by HPLC using a Dynamax C18 column. The resulting peptide was isolated as a single band with no evidence of impurities in high resolution $^1$H-NMR spectra.

### *Preparation of vesicles*

Small unilamellar carboxyfluorescein-entrapped vesicles (phosphatidylcholine:cholesterol, 1:1) were prepared by a sonication method according to published procedures [13,22]. All procedures were performed under argon at ambient temperature, unless stated otherwise. Egg phosphatidylcholine (Sigma) and cholesterol (Sigma) were mixed in a 1:1 stoichiometry in chloroform and the solvent removed under vacuum by rotary evaporation. The lipids were resuspended to 1.5 mM in buffer (80 mM carboxyfluorescein, 10 mM Hepes, pH 7.0, 150 mM NaCl) by vortex mixing, and the resultant lipid dispersion was sonicated for 30 min in a bath type sonicator, and then for 40 min with a probe sonicator (4-mm tip diameter at 20 % power). Metallic debris from the titanium head was removed by centrifugation. Unencapsulated CF was removed by passing the vesicle solution through a Sephadex G-50 column. The lipid concentration of the solution was determined by phosphorus analysis [23]. All vesicle solutions were freshly prepared before each experiment. Negative stain electron microscopy demonstrated the vesicles to be unilamellar with a diameter in the range of 40 ± 10 nm (~60 % had diameters of 40 nm).

### *Fluorescence measurements*

Steady state fluorescence measurements were made on a Perkin Elmer luminescence spectrometer, model LS50B.

### *Carboxyfluorescein release*

A vesicle solution was mixed with a solution of peptide at 25 °C. The reaction buffer contained 10 mM Hepes (pH 7.0) and 150 mM NaCl. For some experiments a pH gradient was used in order to accentuate the amplitude of the spectral change from CF. The pH inside the vesicles was maintained at 5.0 with 10 mM citrate buffer, and the outside pH was 7.0 (10 mM Hepes). The stability of the pH gradient was checked both by monitoring the absorbance of CF inside the vesicles (the absorbance spectrum of CF is highly pH sensitive) and by measuring the pH with a classical pH meter and microelectrode. The pH gradient and the vesicles were stable in the time frame of the experiment. The change in fluorescence signal from CF was monitored as a function of time. Instrument parameters were as follows: carboxyfluorescein, $\lambda_{ex} = 490$ nm, $\lambda_{em} = 520$ nm; slitwidths for excitation and emission were set at 5 nm. The final limiting fluorescence ($F_\infty$) corresponding to 100 % release of carboxyfluorescein was determined by the addition of Triton X-100 (0.02 % final concentration) to the cuvette. This destroys all the vesicles and corresponds to 100 % lysis.

### *Titrations*

Titrations were performed by adding increasing amounts of concentrated vesicle solution to peptide solutions containing 6 μM, 10 μM, 12 μM, and 17 μM peptide. The fluorescence of the tryptophan residue was monitored at equilibrium with $\lambda_{ex} \sim 295$ nm, $\lambda_{em} \sim 355$ nm, and slitwidths of 5 nm for excitation and 10 nm for emission. The contribution of lipid vesicles was independently determined and subtracted from the titration data.

*Acknowledgements:* We thank Dr John Lowbridge of The Ohio State Biochemical Instrument Center for synthesis and purification of the peptide and Kshama Natarajan for NMR analysis. This work was supported by a grant from the donors of the Petroleum Research Fund, administered by the American Chemical Society. N.R. is supported in part by a Lavoisier Fellowship from the Ministère Français des Affaires Etrangères. J.A.C. is a Fellow of the Alfred P. Sloan Foundation, a Camille Dreyfus Teacher-Scholar, and a National Science Foundation Young Investigator.

## References

1. Tschopp, J. & Jongeneel, C.V. (1989). Cytotoxic T lymphocyte mediated cytolysis. In *Perspectives in Biochemistry.* (Neurath, H., ed.), pp. 238–243, American Chemical Society, Washington.
2. Liu, C.-C., Walsh, C.M. & Young, J.D.-E. (1995). Perforin: structure and function. *Immunol. Today* **16**, 194–201.
3. DiScipio, R.G., Gehring, M.R., Podack, E.R., Kan, C.C., Hugli, T.E. & Fey, G.H. (1984). Nucleotide sequence of cDNA and derived amino acid sequence of human complement component C9. *Proc. Natl. Acad. Sci. USA* **81**, 7298–7302.
4. Nagata, S. & Golstein, P. (1995). The Fas death factor. *Science* **267**, 1449–1455.
5. Lowin, B., Hahne, M., Mattmann, C. & Tschopp, J. (1994). Cytotoxic T-cell cytotoxicity is mediated through perforin and Fas lytic pathways. *Nature* **370**, 650.
6. Persechini, P.M., Ojcius, D.M., Adeodato, S.C., Notaroberto, P.C., Daniel, C.B. & Young, J.D.-E. (1992). Channel-forming activity of the perforin N-terminus and a putative α-helical region homologous with complement C9. *Biochemistry* **31**, 5017–5021.
7. Ojcius, D.M., Persechini, P.M., Zheng, L.M., Notaroberto, P.C., Adeodato, S.C. & Young, J.D.-E. (1991). Cytolytic and ion channel-forming properties of the N terminus of lymphocyte perforin. *Proc. Natl. Acad. Sci. USA* **88**, 4621–4625.
8. Lichtenheld, M.G., *et al.*, & Podack, E.R. (1988). Structure and function of human perforin. *Nature* **355**, 448–451.
9. Garland, F. & Christian, S.D. (1975). Thermodynamic and kinetic model of sequential nucleoside base aggregation in aqueous solution. *J. Phys. Chem.* **79**, 1247–1252.
10. Biemann, H.P. & Koshland, D.E. (1994). Aspartate receptors of *Escherichia coli* and *Salmonella typhimurium* bind an aspartate ligand with negative and half-of-the-sites cooperativity. *Biochemistry* **33**, 629–634.
11. Bujalowski, W. & Klonowska, M.M. (1993). Negative cooperativity in the binding of nucleotides to *Escherichia coli* replicative helicase Dna B protein. Interactions with fluorescent nucleotide analogs. *Biochemistry* **32**, 5888–5900.
12. Blumenthal, R., Millard P.J., Henkart M.P., Reynolds C.W. & Henkart, P.A. (1984). Liposomes as targets for granule cytolysin from cytotoxic large granular lymphocyte tumors. *Proc. Natl. Acad. Sci. USA* **81**, 5551–5555.
13. Szoka, F. & Papahadjopoulos, D. (1980). Comparative properties and methods of preparation of lipid vesicles (liposomes). *Annu. Rev. Biophys. Bioeng.* **9**, 467–508.
14. Schwarz, G., Zong, R.T. & Popescu, T. (1992). Kinetics of melittin-induced pore formation in the membrane of lipid vesicles. *Biochim. Biophys. Acta* **1110**, 97–104.
15. Schwarz, G. & Robert, C.H. (1990). Pore formation kinetics in membranes, determined from the release of marker molecules out of liposomes or cells. *Biophys. J.* **58**, 577–583.
16. Schwarz, G. & Beschiaschvili, G. (1989). Thermodynamic and kinetic studies on the association of melittin with a phospholipid bilayer. *Biochim. Biophys. Acta* **979**, 82–90.
17. Palmer, T. (1985). *Understanding Enzymes.* Ellis Horwood, NY.
18. Schwarz, G. Stankowski, S. & Rizzo, V. (1986). Thermodynamic analysis of incorporation and aggregation in a membrane: application to the pore-forming peptide, alamethicin. *Biochim. Biophys. Acta* **861**, 141–151.
19. Rizzo, V., Stankowski, S. & Schwarz, G. (1987). Alamethicin incorporation in lipid bilayers: a thermodynamic study. *Biochemistry* **26**, 2751–2759.
20. Rapaport, D. & Shai, Y. (1991). Interaction of fluorescently labeled pardaxin and its analogs with lipid bilayers. *J. Biol. Chem.* **266**, 23769–23775.
21. Gazit, E. & Shai, Y. (1993). Structural and functional characterization of the α5 segment of *Bacillus thuringiensis* δ-endotoxin. *Biochemistry* **32**, 3429–3436.
22. Woolley, G.A. & Deber, C.M. (1989). A lipid vesicle system for probing voltage-dependent peptide–lipid interactions: application to alamethicin channel formation. *Biopolymers* **28**, 267–272.
23. Bartlett, G.R. (1959). Phosphorus assay in column chromatography. *J. Biol. Chem.* **234**, 466–468.

Received: **28 Aug 1995**; revisions requested: **20 Sept 1995**; revisions received: **14 Nov 1995**. Accepted: **6 Dec 1995**.